JAAS

PAPER

View Article Online
View Journal | View Issue

Cite this: J. Anal. At. Spectrom., 2022, 37, 1722

Theoretical study on signal enhancement of orthogonal double pulse induced plasma

Junxiao Wang,[ab] Yang Zhao,[c] Gang Wang,[d] Lei Zhang, *[ab] Shuqing Wang,[e] Wanfei Zhang,[d] Xiaofei Ma,[d] Zhenrong Liu,[d] Xuebin Luo,[d] Weiguang Ma,[ab] Zefu Ye,[f] Zhujun Zhu,[f] Wangbao Yin*[ab] and Suotang Jia[ab]

Received 25th March 2022
Accepted 17th June 2022

DOI: 10.1039/d2ja00105e

rsc.li/jaas

The double pulse technology increases the energy transmission between the plasma plume and the target by coupling the laser beam, which greatly enhances the signal, reduces the detection limit of laser-induced breakdown spectroscopy (LIBS) and improves the ability of trace elemental analysis. In this paper, the emission characteristics of plasma in orthogonal double-pulse LIBS (DP-LIBS) are studied theoretically by using the hydrodynamics model, including the effects of pulse interval and spot position of the second laser pulse on the emission intensity of various species in the reheating mode. The results show that in the reheating mode, the pulse interval corresponding to the maximum intensity ratio of double pulse to single pulse occurs at 0.2–0.5 μs, while in the pre-ablation mode, it increases with the increase of pulse interval. According to the decrease of the number density of the background gas above the sample before the ablation pulse in the pre-ablation mode, the enhancement mechanism of spectral line intensity is explained from two aspects: plasma–plasma coupling effect and pressure effect. In addition, the spatial distribution and raising mechanism of plasma temperature in these modes are also explored. It shows that in the reheating mode, the plasma temperature is increased by directly absorbing laser energy, while in the pre-ablation mode, it is increased by reducing the energy loss between vapor plasma and gas plasma and weakening the shielding effect. The theoretical analysis of double pulse plasma provides a theoretical basis for the experimental research and application of DP-LIBS.

1. Introduction

Laser-induced breakdown spectroscopy is a plasma spectroscopy technology developed in recent decades for qualitative and quantitative analysis of sample components. Due to its advantages of being fast and suitable for all kinds of materials, and simultaneous detection of multiple elements, it has been widely used in environmental monitoring,[1–3] cultural relics protection and archaeological science,[4–6] space exploration[7–9] and other fields. However, its detection sensitivity is poor, especially the detection limits of several elements are difficult to meet the application requirements of trace analysis.[10] In order to improve the detection sensitivity of LIBS, a variety of auxiliary spectral enhancement techniques have been developed in recent years, including double/multi-pulse re-excitation,[11–16] discharge/microwave assisted enhancement,[17,18] space/magnetic field constrained plasma,[19,20] laser-induced fluorescence,[21,22] *etc.* Among them, DP-LIBS is the most widely used technique in enhancing the spectrum by re-exciting the plasma with a secondary laser pulse. Since E. H. Piepmeier and H. V. Malmstadt first proposed the concept of DP-LIBS in 1969,[23] this technique has attracted the interest of more researchers. Currently reported laser wavelength covers infrared,[11–16,24,25] visible and even ultraviolet,[26] and the laser pulse width ranges from nanosecond[11–16,26] to femtosecond.[27] DP-LIBS has been proved to not only enhance the spectral line intensity by 1.5–33 times,[24,27] but also significantly improve the spectral signal-to-noise ratio (SNR),[11] thereby reducing the detection limit by several times or even one magnitude.[28,29] According to the optical structure, DP-LIBS is divided into collinear configuration[11,25,26] and orthogonal configuration.[12–16,24,27] Although the former can use a single double-pulse laser source, it is difficult to independently control the plume ablation and excitation process, while the latter can be flexibly adjusted to facilitate the study of the enhancement mechanism of double-pulse spectrum, the radiation characteristics and kinetic expansion process of the plasma.[16] The orthogonal DP-LIBS can be further

[a]State Key Laboratory of Quantum Optics and Quantum Optics Devices, Institute of Laser Spectroscopy, Shanxi University, Taiyuan, China. E-mail: k1226@sxu.edu.cn; ywb65@sxu.edu.cn

[b]Collaborative Innovation Center of Extreme Optics, Shanxi University, Taiyuan, China

[c]School of Science, North University of China, Taiyuan, China

[d]Shanxi Xinhua Chemical Defense Equipment Research Institute Co., Ltd, Taiyuan, China

[e]National Energy R&D Center of Petroleum Refining Technology (RIPP, SINOPEC), Beijing, China

[f]Shanxi Gemeng US-China Clean Energy R&D Center Co., Ltd, Taiyuan, China

divided into reheating and pre-ablation modes according to the action sequence of the two laser beams. In the reheating mode, the initial plasma is induced by the laser perpendicular to the sample surface and then reheated by the other laser beam (Fig. 1a). In the pre-ablation mode, the laser parallel to the sample surface first breaks through the ambient gas to induce the initial plasma, and then the other laser ablates the focal spot on the sample surface (Fig. 1b).

For decades, in addition to experimental studies, a large number of theoretical studies on DP-LIBS have also been carried out. For example, A. Casavola *et al.* studied the double pulse plasma under water by combining the bubble dynamics code and the Euler equations describing the plasma evolution. They pointed out that the LIBS signal depended on the bubble conditions in which the plasma was generated, and that inter-pulse delay changed the plasma parameters and the effects of the chemical reaction.[30] V. N. Rai *et al.* considered that plasma emission is proportional to the square of the density, volume and fraction of the second laser pulse absorbed by the plasma, and studied the evolution of enhancement with pulse interval and delay time under different conditions by using a simplified model. They found that the increase of mass ablated from the target after the second laser pulse played a dominant role in the enhancement.[31] L. Fornarini *et al.* assumed that the plasma was homogeneous and expanded with the electron temperature of the target as well as the concentration obtained through the evaporation flux. They studied the plasma parameters and ablation depth under different combinations and found that the fs ns^{-1} laser source was more likely to meet the local thermal equilibrium conditions.[32] X. Zhao *et al.* investigated the plasma produced by a double pulse induced silicon target using an atomistic model including the molecular dynamics method, the Monte Carlo method, the particle-in-cell method, and the beam propagation method. Through the relationship between ablation depth and pulse delay, they proposed different ablation enhancement mechanisms under different pulse delays.[33] V. B. Fokin *et al.* calculated the electron temperature of femtosecond double pulse plasma and the ablation depth of the target by using the hydrodynamic two-temperature model and the molecular dynamic two-temperature model respectively, and obtained quite similar results.[34] A. Alberti *et al.* applied two-temperature Navier–Stokes equations to the pre-ablation mode combining ultraviolet and infrared pulses, compared the plasma parameters generated at different focal points of the infrared pulse, and found that there would be more absorption when the focal points overlapped.[35] U. P. Padhi *et al.* used the Navier–Stokes equations to simulate the evolution of plasma parameters under long and short pulse intervals, and concluded that a single pulse can be replaced by a double pulse with the same total energy and short pulse interval.[36] All the above theoretical studies on the double pulse were carried out in the collinear configuration. Because the collinear and orthogonal structures are different, the signal enhancement mechanisms are also different. In the orthogonal double pulse, the increase of mass ablated from the sample caused by the laser pulse parallel to the sample is usually ignored, which leads to signal enhancement. Different modes of orthogonal DP-LIBS involve different processes, and the physical reasons for the signal enhancement are relatively complex. Moreover, the action sequence of the two laser pulses, pulse interval and the focusing position of the laser relative to the sample surface have important influences on the signal enhancement. The above experimental tests are time-consuming and involve heavy workload. It is necessary to analyze the source of signal enhancement of orthogonal DP-LIBS more deeply and simply through theoretical simulation.

In this work, the plasmas generated in the orthogonal DP-LIBS configuration in both reheating and pre-ablation modes were numerically simulated, and the fluorescence characteristics, electron temperature and signal enhancement mechanisms were studied.

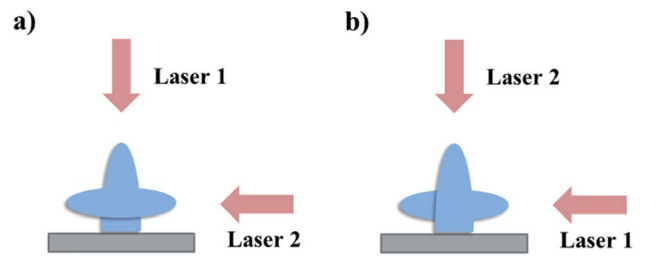

Fig. 1 Schematic diagrams of reheating (a) and pre-ablation (b) modes in orthogonal DP-LIBS.

2. Description of the theoretical model

When a laser beam acts on a sample, heat conduction is the main heat transfer mechanism to transfer the laser energy from the sample surface to its interior, so the heating process is usually described by the heat conduction equation. The one-dimensional heat conduction equation is:

$$c_p\rho_t\left[\frac{\partial T_t}{\partial t}-v\frac{\partial T_t}{\partial z}\right]=\lambda_t\frac{\partial^2 T_t}{\partial z^2}+(1-R)\alpha_t I_t\exp(-\alpha_t z), \quad (1)$$

where c_p, ρ_t, λ_t, R, and α_t are the properties of the target, corresponding to specific heat, mass density, thermal conductivity, reflectivity and absorption coefficient, T_t and v are respectively the temperature and evaporation rate of the target, I_t is the laser power density reaching the target surface, z is the coordinate along the inward normal to the target surface, and ∂ is the partial derivative symbol.

The ablated area is heated to the boiling point to produce vapor, which will continue to absorb energy and ionize to form a vapor plasma, pushing the surrounding ambient gas to expand outward. This expansion process can be described by the two-dimensional axisymmetric hydrodynamics equations involving the interaction term between vapor plasma and background gas:[37]

$$\frac{\partial\rho_i}{\partial t}+\nabla\cdot(\rho_i(\vec{u}+\vec{u}_{d_i}))=0, \quad (2)$$

$$\frac{\partial \rho \vec{u}}{\partial t} + \nabla \cdot (\rho \vec{u}\vec{u}) = \nabla \cdot \tau - \nabla p, \quad (3)$$

$$\frac{\partial \rho \left(e + \frac{\vec{u}^2}{2} \right)}{\partial t} + \nabla \cdot \left(\rho \left(e + \frac{\vec{u}^2}{2} \right) \vec{u} \right) = \nabla (\tau \cdot \vec{u}) - \nabla \cdot (p\vec{u}) + \nabla \cdot (\lambda \nabla T) + (\alpha_{IB} + \alpha_{PI}) I_t - q, \quad (4)$$

where ρ_i and u_{d_i} correspond to the mass density, diffusion velocity of i species, ρ, u, T are respectively the total mass density, velocity and plasma temperature, p and e are the local pressure and specific internal energy obtained by combining the equation of state of ideal gas, τ, λ, α_{IB}, and α_{PI} are the viscous stress tensor, thermal conductivity, inverse bremsstrahlung absorption coefficient and photoionization coefficient, q is the radiation power loss, and ∇ is the gradient operator.

Through the boundary conditions of the Knudsen layer and the balance conditions on the sample surface, the hydrodynamics model can be coupled with the heat conduction model to obtain the sample surface temperature, evaporation rate, and initial plasma parameters, including total number density, velocity, and plasma temperature. Combined with Saha equation and the charge conservation equation, the number density of each atom and ion can be obtained.

Based on the plasma parameters obtained through hydrodynamics equations, the emission intensity of species in the plasma under local thermal equilibrium is:

$$I = hcN \frac{gB}{\lambda U} \exp\left(-\frac{E}{k_B T} \right), \quad (5)$$

where N is the species number density, U is the partition function, B, λ, g, and E are the transition probability, wavelength, degeneracy and energy of the upper energy level, and h, c, and k_B are the Planck constant, the speed of light and the Boltzmann constant.

In this work, the orthogonal double-pulse laser-induced plasma produced from an Al–Mg alloy in argon at atmospheric pressure was simulated by using the above model. Here, the pulse width of Gaussian laser is 10 ns and the peak power density is 2×10^9 W cm^{-2}, and the parameters of the alloy at room temperature are listed in Table 1. The emission characteristics of vapor species (Mg I, Mg II, Al I, Al II) and background gas species (Ar I, Ar II) in plasma were analyzed. The spectroscopic parameters of each species listed in Table 2 are from the NIST database.

Table 1 Physical parameters of the Al–Mg alloy

Parameters	Values
Specific heat, c_p (J g^{-1} K^{-1})	0.90
Mass density, ρ_t (g cm^{-3})	2.7
Thermal conductivity, λ_t (W cm^{-1} K^{-1})	2.37
Reflectivity, R	0.90
Absorption coefficient, α_t (cm^{-1})	1.5×10^6
Melting point, T_m (K)	921 (Mg), 934 (Al)
Boiling point, T_b (K)	1363 (Mg), 2792 (Al)

3. Results and discussion

3.1 Orthogonal reheating DP-LIBS

In order to intuitively understand the evolution of spectral line intensity with delay time after laser irradiation, Fig. 2 shows the temporal evolution of Al II 358.66 nm line intensity with single LIBS and orthogonal reheating DP-LIBS at different pulse intervals. The gray line represents the evolution curve after the action of a single pulse, while the others represent the evolution curves after the action of the second laser in the double pulse configuration. The temporal evolution of the spectral line intensity after the action of the first laser in the double pulse configuration is the same as that under the single pulse. It can be seen that after the action of the laser pulse, the spectral line intensity reaches the maximum rapidly, and then decreases slowly. Compared with the single pulse, the evolution curves of the double pulse have two peaks, and under each delay, the spectral line intensity increases in different degrees due to the action of the reheating pulse. When the spot position of the second laser is close to the central region of the plasma, the spectral line intensity increases with the rise of plasma temperature after the reheating pulse. Because the spot position is close to the target, when the pulse interval is small, the heating region is located in the center of the plasma; in contrast, when the pulse interval is large it is located in the tail

Table 2 Spectroscopic parameters of the characteristic spectral lines of various species

Species	λ_{ul} (nm)	A_{ul} ($\times 10^7$ s^{-1})	E_u (eV)
Mg I	518.36	5.61	5.11
Mg II	448.11	23.30	11.63
Al I	396.15	9.85	3.14
Al II	358.66	23.50	15.30
Ar I	763.51	2.45	13.17
Ar II	484.78	8.49	19.31

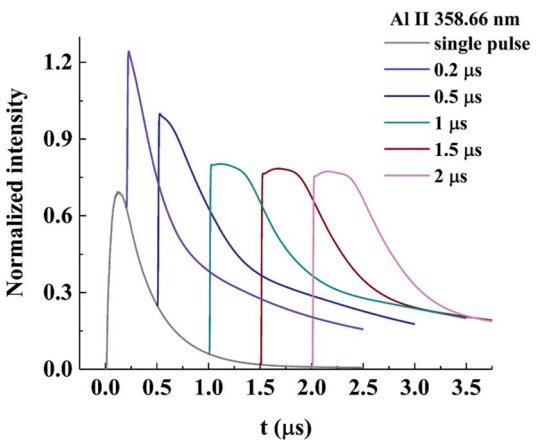

Fig. 2 Temporal evolution of Al II spectral line intensity with single LIBS and orthogonal reheating DP-LIBS at different pulse intervals (energy of two laser beams: 100 mJ, distance between the center of the second laser spot and the sample surface: 1 mm).

of the plasma. Therefore, the peak intensity after the action of the second pulse first increases and then decreases with the pulse interval, and the maximum peak appears at the pulse interval of 0.2 μs. To verify the above explanation, the spatial evolution of temperature on the symmetry axis of the plasma with different delays in the single pulse configuration is shown in Fig. 3. When the peak intensity reaches the maximum, the corresponding pulse interval is approximately equal to the time when the central region of the plasma reaches the spot position of the second laser in the double pulse configuration.

Fig. 2 qualitatively shows that the pulse interval will affect the spectral line intensity, and Fig. 4 further quantitatively shows the temporal evolution of line intensity ratio of each species with the pulse interval in the reheating configuration. The delay time of different species is different, corresponding to the value when the intensity reaches the optimal value in the single pulse mode. For Mg I, Mg II, Al I, Al II, Ar I, the delay time is 214 ns, 118 ns, 158 ns, 133 ns, and 289 ns. The vertical axis represents the intensity ratio after the action of the second laser in the double pulse configuration to that after the action of a single pulse. The intensity ratio depends on the characteristics of the selected spectral lines. The values of all species first increase rapidly and then decrease with the pulse interval, and the peak appears at 0.2 μs to 0.5 μs. The maximum signal enhancement with different experimental parameters corresponds to different pulse intervals. C. Gautier *et al.* found that for ionic lines and atomic lines with high excitation energy level, the optimal pulse interval was 200 ns.[38] Our theoretical optimal pulse interval is similar to this experimental result. However, R. Sanginés *et al.* observed that the signal enhancement of atomic lines reached the maximum a few microseconds after the second laser.[15] In addition, within the range of pulse interval studied, the enhancement factors of ionic lines are much greater than those of atomic lines, which will be discussed in detail.

According to the intensity formula and combined with Saha equation, the emission intensity of atomic and ionic lines is:[12]

$$I_{\mathrm{I}} = \frac{hcB_{\mathrm{I}}g_{\mathrm{I}}N_0}{\lambda_{\mathrm{I}}U_0}\exp\left(-\frac{E_{\mathrm{I}}}{k_{\mathrm{B}}T}\right), \tag{6}$$

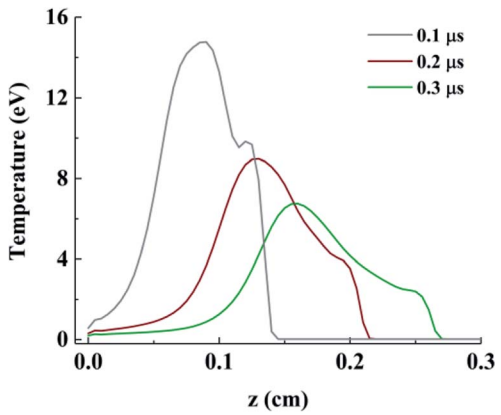

Fig. 3 Spatial distribution of temperature on the symmetry axis of the plasma at different delays in the single pulse configuration.

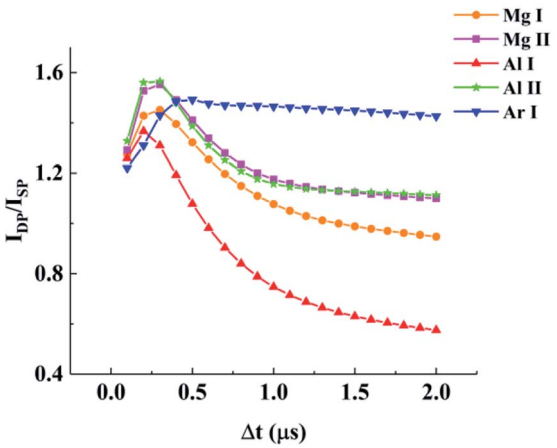

Fig. 4 Temporal evolution of the line intensity ratio of each species with the pulse interval in the reheating configuration (energy of the two laser beams: 100 mJ, distance between the center of the second laser spot and the sample surface: 1 mm).

$$I_{\mathrm{II}} = \frac{hcB_{\mathrm{II}}g_{\mathrm{II}}N_0}{\lambda_{\mathrm{II}}U_0}\frac{2(2\pi m_{\mathrm{e}}k_{\mathrm{B}})^{3/2}}{h^3}\frac{T^{3/2}}{N_{\mathrm{e}}}\exp\left(-\frac{E_{\mathrm{II}}+E_{\mathrm{IP}}}{k_{\mathrm{B}}T}\right), \tag{7}$$

where m_{e} is the mass of the electron, N_0 and N_{e} are the atomic number density and electron number density, U_0 is the partition function of an atom, and E_{IP} is the ionization potential.

For the same transition, the intensity ratio of spectral lines can be expressed as:

$$\frac{I_{\mathrm{I,DP}}}{I_{\mathrm{I,SP}}} = \frac{N_{0,\mathrm{DP}}U_{0,\mathrm{SP}}}{N_{0,\mathrm{SP}}U_{0,\mathrm{DP}}}\exp\left(-\frac{1}{k_{\mathrm{B}}}\left(\frac{1}{T_{\mathrm{DP}}}-\frac{1}{T_{\mathrm{SP}}}\right)\times E_{\mathrm{k}}^{*}\right), \tag{8}$$

$$\frac{I_{\mathrm{II,DP}}}{I_{\mathrm{II,SP}}} = \frac{N_{0,\mathrm{DP}}U_{0,\mathrm{SP}}}{N_{0,\mathrm{SP}}U_{0,\mathrm{DP}}}\frac{T_{\mathrm{DP}}^{3/2}}{T_{\mathrm{SP}}^{3/2}}\frac{N_{\mathrm{e,SP}}}{N_{\mathrm{e,DP}}}\exp\left(-\frac{1}{k_{\mathrm{B}}}\left(\frac{1}{T_{\mathrm{DP}}}-\frac{1}{T_{\mathrm{SP}}}\right)\times E_{\mathrm{k}}^{*}\right), \tag{9}$$

where E_{k}^{*} is the excitation energy level, $E_{\mathrm{k}}^{*}=E_{\mathrm{k}}^{\mathrm{I}}$ is for atomic lines, and $E_{\mathrm{k}}^{*}=E_{\mathrm{k}}^{\mathrm{II}}+E_{\mathrm{IP}}$ is for ionic lines.

In the reheating DP-LIBS mode, considering that the reheating pulse no longer ablates the target, the change of electron number density caused by plasma expansion can be ignored when the pulse interval is small. The logarithmic transformation of both sides of eqn (6) gives the expression $\ln\frac{I_{\mathrm{I}}\lambda_{\mathrm{I}}}{B_{\mathrm{I}}g_{\mathrm{I}}} = -\frac{E_{\mathrm{I}}}{k_{\mathrm{B}}T}+\ln\left(\frac{hcN_0}{U_0}\right)$, and the temperature can be obtained from the slope of the linear fitting. Six Mg I lines were used to calculate the average temperatures in the double pulse and single pulse configurations, which are 3.09 eV and 2.99 eV respectively. Since the effect of $(T_{\mathrm{DP}}/T_{\mathrm{SP}})^{3/2}$ on the signal enhancement is much smaller than that of the exponential term and can be ignored, the intensity ratio of spectral lines can be simplified as:

$$\frac{I_{\mathrm{DP}}}{I_{\mathrm{SP}}} = A\exp\left(B\times E_{\mathrm{k}}^{*}\right), \tag{10}$$

where $A=\frac{N_{0,\mathrm{DP}}U_{0,\mathrm{SP}}}{N_{0,\mathrm{SP}}U_{0,\mathrm{DP}}}$, $B=\left(-\frac{1}{k_{\mathrm{B}}}\left(\frac{1}{T_{\mathrm{DP}}}-\frac{1}{T_{\mathrm{SP}}}\right)\right)$

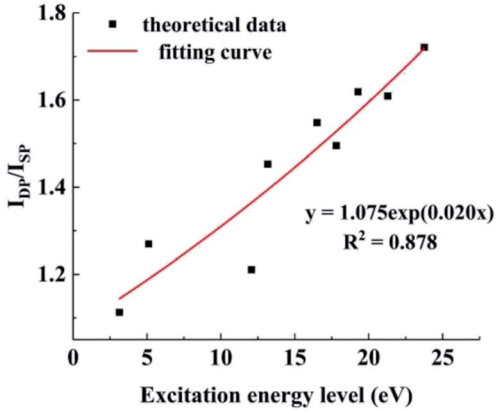

Fig. 5 Relationship between the line intensity ratio and excitation energy level (energy of two laser beams: 100 mJ, distance between the center of the second laser spot and the sample surface: 1 mm, pulse interval: 0.5 μs, delay time: 0.3 μs).

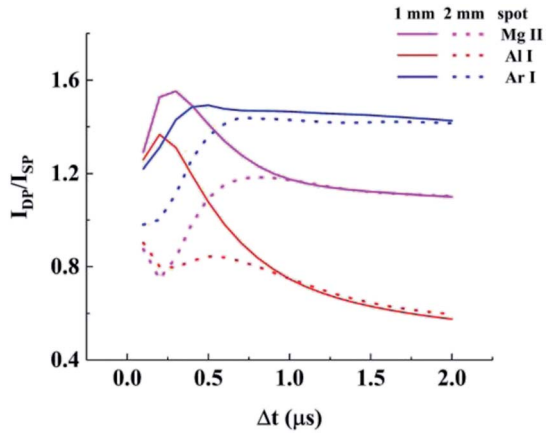

Fig. 6 Temporal evolution of line intensity ratio with pulse interval at different spot positions and delays (energy of two laser beams: 100 mJ).

Fig. 5 shows the relationship between the intensity ratio of spectral lines and excitation energy level at a pulse interval of 0.5 μs, where the solid square represents the theoretical data and the solid line is the fitting curve with R^2 greater than 0.87. This shows that the relationship can be approximately expressed by an exponential function, and well explains the phenomenon in Fig. 4 that the intensity ratio increases with the excitation energy level at the short pulse interval. C. Gautier *et al.*[12] and Q. Wang *et al.*[39] also pointed out that in the reheating DP-LIBS mode with a short pulse interval, the signal enhancement has a similar exponential growth trend with the increase of excitation energy level. This exponential relationship is also applicable to the signal enhancement of femtosecond double-pulse plasma, which has been used to explain the difference of signal enhancement of atomic and ionic lines in orthogonal femtosecond DP-LIBS.[40]

The spot position of the second laser also affects the intensity ratio of spectral lines, and Fig. 6 depicts the relationship between the intensity ratio and pulse interval at different spot positions. The spot centers of the second laser corresponding to the solid line and the dotted line are located at 1 mm and 2 mm respectively. At the same delay time, the pulse interval affects the signal enhancement. For a short pulse interval, the lower the spot position, the greater the signal is enhanced. However, for the long pulse interval, the spot position has little effect on signal enhancement. At the same time, the pulse interval is also related to the position where the plasma is heated by the laser after expansion, that is, when the central region of the plasma is close to the spot of the second laser, the signal is also greatly enhanced.

3.2 Orthogonal pre-ablation DP-LIBS

We also studied the relationship between the intensity ratio of spectral lines and the pulse interval in the pre-ablation mode, and the results are shown in Fig. 7. The delay time in the single mode corresponds to the maximum line intensity, which is 104 ns for Ar II. It can be seen that the line intensity ratio basically increases with the increase of pulse interval. Combined with Fig. 4, it can be concluded that in the case of the small pulse interval, reheating can more significantly enhance the signal, otherwise the performance of pre-ablation is better. Similar to the relationship in the orthogonal reheating mode, the intensity ratio in the orthogonal pre-ablation mode is also closely related

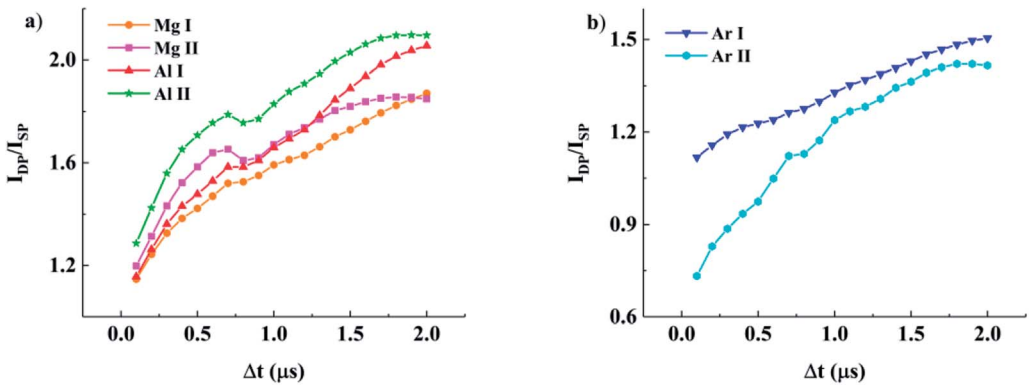

Fig. 7 Relationship between the intensity ratio of vapor species (a) and argon species (b) and pulse interval in the pre-ablation mode (energy of two laser beams: 100 mJ, distance between the center of the second laser spot and the sample surface: 1 mm).

to the upper energy levels of the selected spectral lines, that is, the higher the upper energy level, the more significantly the signal is enhanced. In the pulse interval studied, the vapor species intensity ratio of double pulse to single pulse is greater than 1, indicating that the orthogonal pre-ablation double pulse always further enhances the signal of the single pulse. As for signal enhancement in the orthogonal pre-ablation mode, the main mechanisms include plasma–plasma coupling, and pressure and heating effects of the plasma on the sample,[41] which have been confirmed by many experiments.[13,14,16,41] The enhancement mechanisms are basically the same as that in the collinear pre-ablation mode. In ref. 41, J. Scaffidi *et al.* observed the decrease of gas species intensity in the orthogonal femtosecond–nanosecond configuration, which was associated with the increase of ablative species intensity. Similarly, A. Safi *et al.* found that the air species intensity ratio of double pulse to single pulse was always less than 1 in the orthogonal nanosecond double pulse configuration.[16] They explained the intensity decrease of background gas and the intensity increase of ablative species by using the pressure effect, that is, the low pressure or low concentration region was formed above the sample. However, Fig. 7b shows that in theory, the gas species intensity of the double pulse is still larger than that of the single pulse. The difference between theoretical simulation and experimental results is mainly due to the significant increase of plasma temperature, which will be explained later.

In the pre-ablation mode, the number density of background gas above the sample decreases before the arrival of the second laser. Fig. 8 shows the temporal evolution of the number density of background gas after the action of pre-ablation pulse and the contour diagrams of number density at four delays. The results show that the number density of argon species in the central region is significantly lower than that in the surrounding region. The number density of the central region decreases with the outward expansion of the plasma, while the low number density region expands gradually. The vapor plasma generated by the second laser in the pre-ablation mode has lower density and higher temperature than those of the plasma induced by the single pulse under argon gas at one atmosphere pressure. From the perspective of the plasma–plasma coupling effect, such an environment makes the energy and heat conduction loss caused by the collision between vapor plasma and gas species smaller, so as to realize signal enhancement. In terms of the pressure effect, the reduction of gas species density weakens the shielding effect, improves the coupling efficiency between the laser and the sample, increases the ablation mass of the sample, and enhances the spectral signal. As in ref. 13, G. Cristoforetti *et al.* found that the trend of double pulse and low-pressure single pulse was consistent by comparing the samples ablated by double pulse at atmospheric pressure and single pulse at different pressures, which directly proved that the low-pressure environment of plasma generated by the second laser, *i.e.*, the weak shielding effect, was one of the factors of signal enhancement. In addition, since the direct heating of the sample will hardly enhance the signal in the double pulse configuration,[42] the contribution of the gaseous plasma heating to the signal enhancement is ignored in this work.

Temperature is an important parameter to characterize the plasma, which directly affects its fluorescence characteristics. Fig. 9 shows the isolines of plasma temperature under different experimental conditions, and gives the evolution diagram of plasma temperature in the single pulse configuration for comparison. As can be seen, in the single pulse configuration, the plasma is a symmetrical arch, while in the double pulse configuration, the plasma presents asymmetry. The plasma asymmetry in the pre-ablation mode is not easy to be observed, but it is obvious in the reheating mode. When the reheating pulse is 1 mm away from the sample surface, the high-temperature region of the plasma shows discontinuity. When the distance between the spot position of the second laser and sample surface is 2 mm, the high temperature region of the plasma shifts to the right. This is because the second laser is incident from the right side of the plasma, so this side absorbs more laser energy. For the orthogonal double pulse, the plasma temperature is higher than that of the single pulse under the same conditions, whether in the pre-ablation or reheating mode. Taking the 0.3 μs delay and 1 mm spot position as an example, the average temperature in the single pulse configuration is 2.99 eV, while in the pre-ablation and reheating modes, it is 3.54 eV and 3.09 eV, respectively. Compared with the single pulse, the temperature in the pre-ablation mode increases significantly. The influence of the exponential term in eqn (10) is greater than that of $(N_{0,DP}U_{0,SP})/(N_{0,SP}U_{0,DP})$, so the intensity ratio of background gas species obtained in Fig. 7b is greater than 1. The difference of plasma temperature profile implies that the rising mechanisms of plasma temperature in the two modes are different. In the pre-ablation mode, the temperature increases by means of the coupling effect of vapor plasma and gas plasma, but in the reheating mode, it increases due to the absorption of laser energy by vapor plasma.

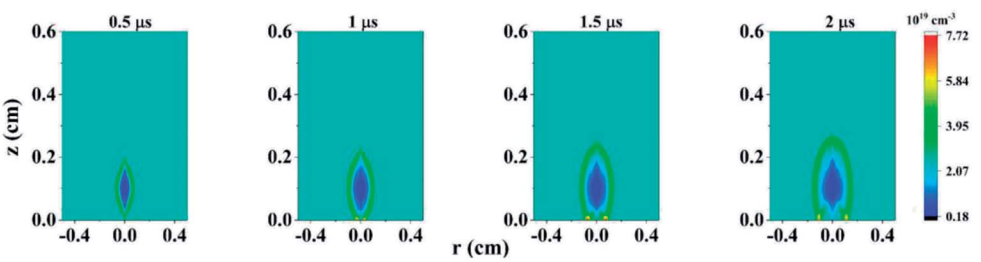

Fig. 8 Temporal evolution of the number density of argon species after pre-ablation.

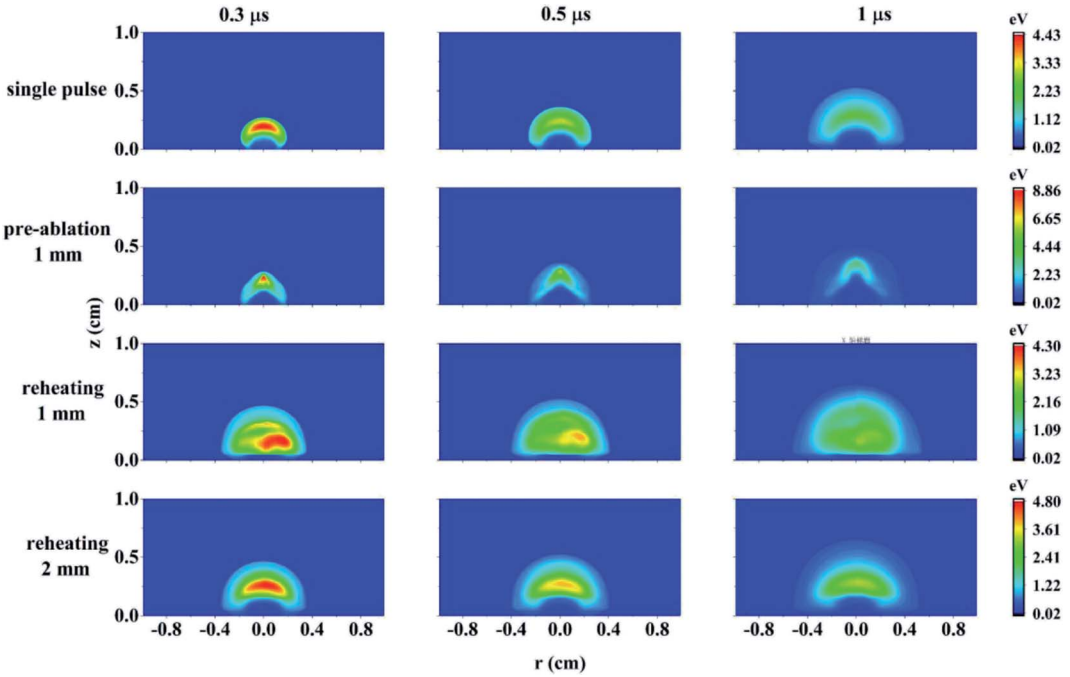

Fig. 9 Temporal evolution of plasma temperature under different experimental conditions (energy of two laser beams: 100 mJ, pulse interval: 0.5 μs).

4. Conclusion

In this paper, the evolution of line intensity ratios of species in the orthogonal double pulse configuration was studied by using the hydrodynamic model. Firstly, by comparing the influence of the pulse interval on the intensity ratio in different modes, it was found that reheating is a better signal enhancement mode when the interval is short; in contrast, the pre-ablation mode is better. Secondly, we studied the effect of the spot position of the second laser on signal enhancement in the reheating mode. When the center region of the expanding plasma is close to the laser spot, the spectrum will be greatly enhanced. Finally, according to the evolution of the number density of background gas and the comparison of the plasma temperature profiles in the two modes, the various possible mechanisms of signal enhancement were discussed. In the reheating mode, the plasma directly absorbs the laser energy to increase the temperature and enhance the radiation. In the pre-ablation mode, considering the reduction of the number density of background gas above the sample, the radiation is enhanced by the decrease of energy loss between vapor plasma and gas plasma and the increase of ablation mass. The theoretical simulation of the evolution of the plasma formed by DP-LIBS fully confirms the previous explanation of the enhancement mechanisms in the double pulse experiments.

Author contributions

J. X. W. was the main author and responsible for the first draft of the manuscript. All authors provided their reviews and comments on the subsequent versions of the manuscript. J. X. W. was responsible for theoretical simulations, acquisition of theoretical data and analysis of results. Y. Z. and L. Z. arranged the structure of the manuscript and modified it appropriately. G. W., S. Q. W. and W. G. M. explained the results and provided suggestions to improve the manuscript. W. F. Z., X. F. M., Z. R. L. and X. B. L. provided guidance to theoretical models. Z. F. Y., Z. J. Z., W. B. Y. and S. T. J. have provided support with the model setup, analysis, and interpretation of results. All authors read and approved the final manuscript.

Conflicts of interest

There are no conflicts of interest to declare.

Acknowledgements

National Key R&D Program of China (2017YFA0304203); National Energy R&D Center of Petroleum Refining Technology (RIPP, SINOPEC); Changjiang Scholars and Innovative Research Team in University of Ministry of Education of China (IRT_17R70); National Natural Science Foundation of China (NSFC) (61975103, 61875108, 627010407); 111 Project (D18001); Fund for Shanxi "1331KSC".

References

1 X. Yu, L. Yang, X. Gu, J. Bao, H. Yang and L. Sun, *Environ. Monit. Assess.*, 2014, **186**, 8969–8980.
2 L. F. Viana, Y. R. Súarez, C. A. L. Cardoso, S. M. Lima, L. H. D. C. Andrade and S. E. Lima-Junior, *Chemosphere*, 2019, **228**, 258–263.

3 Y. Zhang, T. Zhang and H. Li, *Spectrochim. Acta, Part B*, 2021, **181**, 106218.
4 A. Giakoumaki, K. Melessanaki and D. Anglos, *Anal. Bioanal. Chem.*, 2007, **387**, 749–760.
5 A. Botto, B. Campanella, S. Legnaioli, M. Lezzerini, G. Lorenzetti, S. Pagnotta, F. Poggialini and V. Palleschi, *J. Anal. At. Spectrom.*, 2019, **34**, 81–103.
6 Y. Yin, D. Sun, Z. Yu, M. Su, Z. Shan, B. Su and C. Dong, *J. Cult. Herit.*, 2021, **47**, 109–116.
7 A. K. Knight, N. L. Scherbarth, D. A. Cremers and M. J. Ferris, *Appl. Spectrosc.*, 2000, **54**, 331–340.
8 R. Shu, W. Xu, Z. Fu, X. Wan and R. Yuan, *Journal of Deep Space Exploration*, 2018, **5**, 450–457.
9 S. Kubitza, S. Schröder, E. Dietz, S. Frohmann, P. B. Hansen, K. Rammelkamp, D. S. Vogt, M. Gensch and H. W. Hübers, *Spectrochim. Acta, Part B*, 2020, **174**, 105990.
10 J. D. Winefordner, I. B. Gornushkin, T. Correll, E. Gibb, B. W. Smith and N. Omenetto, *J. Anal. At. Spectrom.*, 2004, **19**, 1061–1083.
11 R. Sattmann, V. Sturm and R. Noll, *J. Phys. D: Appl. Phys.*, 1995, **28**, 2181–2187.
12 C. Gautier, P. Fichet, D. Menut, J. L. Lacour, D. L'Hermite and J. Dubessy, *Spectrochim. Acta, Part B*, 2005, **60**, 265–276.
13 G. Cristoforetti, *Spectrochim. Acta, Part B*, 2009, **64**, 26–34.
14 R. Sanginés and H. Sobral, *J. Appl. Phys.*, 2011, **110**, 033301.
15 R. Sanginés, V. Contreras, H. Sobral and A. Robledo-Martinez, *Spectrochim. Acta, Part B*, 2015, **110**, 139–145.
16 A. Safi, M. Bahreini and S. H. Tavassoli, *Opt. Spectrosc.*, 2016, **120**, 367–378.
17 M. Tampo, M. Miyabe, K. Akaoka, M. Oba, H. Ohba, Y. Maruyama and I. Wakaida, *J. Anal. At. Spectrom.*, 2014, **29**, 886–892.
18 M. Pérez-Rodríguez, P. M. Dirchwolf, T. V. Silva, A. L. Vieira, J. A. G. Neto, R. G. Pellerano and E. C. Ferreira, *Food Chem.*, 2020, **331**, 127051.
19 L. B. Guo, W. Hu, B. Y. Zhang, X. N. He, C. M. Li, Y. S. Zhou, Z. X. Cai, X. Y. Zeng and Y. F. Lu, *Opt. Express*, 2011, **19**, 14067–14075.
20 J. Guo, T. Wang, J. Shao, A. Chen and M. Jin, *J. Anal. At. Spectrom.*, 2018, **33**, 2116–2123.
21 S. L. Lui, Y. Godwal, M. T. Taschuk, Y. Y. Tsui and R. Fedosejevs, *Anal. Chem.*, 2008, **80**, 1995–2000.
22 L. B. Guo, Z. H. Zhu, J. M. Li, Y. Tang, S. S. Tang, Z. Q. Hao, X. Y. Li, Y. F. Lu and X. Y. Zeng, *Opt. Express*, 2018, **26**, 2634–2642.
23 E. H. Piepmeier and H. V. Malmstadt, *Anal. Chem.*, 1969, **41**, 700–707.
24 D. N. Stratis, K. L. Eland and S. M. Angel, *Appl. Spectrosc.*, 2000, **54**, 1270–1274.
25 R. Hai, P. Liu, D. Wu, H. Ding, J. Wu and G. N. Luo, *Fusion Eng. Des.*, 2014, **89**, 2435–2439.
26 L. St-Onge, V. Detalle and M. Sabsabi, *Spectrochim. Acta, Part B*, 2002, **57**, 121–135.
27 J. Scaffidi, J. Pender, W. Pearman, S. R. Goode, B. W. Colston, J. C. Carter and S. M. Angel, *Appl. Opt.*, 2003, **42**, 6099–6106.
28 M. A. Ismail, G. Cristoforetti, S. Legnaioli, L. Pardini, V. Palleschi, A. Salvetti, E. Tognoni and M. A. Harith, *Anal. Bioanal. Chem.*, 2006, **385**, 316–325.
29 A. S. Zakuskin, A. M. Popov, S. M. Zaytsev, N. B. Zorov, M. V. Belkov and T. A. Labutin, *J. Appl. Spectrosc.*, 2017, **84**, 319–323.
30 A. Casavola, A. D. Giacomo, M. Dell'Aglio, F. Taccogna, G. Colonna, O. D. Pascale and S. Longo, *Spectrochim. Acta, Part B*, 2005, **60**, 975–985.
31 V. N. Rai, F. Y. Yueh and J. P. Singh, *Appl. Opt.*, 2008, **47**, 30–37.
32 L. Fornarini, R. Fantoni, F. Colao, A. Santagata and R. Teghil, *AIP Conf. Proc.*, 2009, **1172**, 59–66.
33 X. Zhao and Y. C. Shin, *Appl. Phys. Lett.*, 2014, **105**, 111907.
34 V. B. Fokin, M. E. Povarnitsyn and P. R. Levashov, *Appl. Surf. Sci.*, 2017, **396**, 1802–1807.
35 A. Alberti, A. Munafò, C. Pantano, J. B. Freund and M. Panesi, *J. Phys. D: Appl. Phys.*, 2020, **53**, 205202.
36 U. P. Padhi, A. P. Singh and R. Joarder, *Int. J. Heat Fluid Flow*, 2020, **82**, 108563.
37 J. Wang, S. Wang, L. Zhang, M. Su, D. Sun, Q. Min, W. Ma, W. Yin and S. Jia, *Plasma Sci. Technol.*, 2022, **24**, 035005.
38 C. Gautier, P. Fichet, D. Menut, J. L. Lacour, D. L'Hermite and J. Dubessy, *Spectrochim. Acta, Part B*, 2004, **59**, 975–986.
39 Q. Wang, J. Wang, Y. Liang, X. Chen, B. Wu, Z. Ni and F. Dong, *Proc. SPIE*, 2011, **8201**, 82012I.
40 X. Liu, S. Sun, X. Wang, Z. Liu, Q. Liu, P. Ding, Z. Guo and B. Hu, *Opt. Express*, 2013, **21**, A704–A713.
41 J. Scaffidi, W. Pearman, M. Lawrence, J. C. Carter, B. W. Colston Jr and S. M. Angel, *Appl. Opt.*, 2004, **43**, 5243–5250.
42 J. Register, J. Scaffidi and S. M. Angel, *Appl. Spectrosc.*, 2012, **66**, 869–874.